Infrared Physics and Technology 99 (2019) 80–85

Contents lists available at ScienceDirect

Infrared Physics & Technology

journal homepage: www.elsevier.com/locate/infrared

Regular article

Laser damage characteristics of indium-tin-oxide film and polyimide film

Xiaofeng Liu[a,b], Liping Peng[a,b,c], Yanqi Gao[d], Yuan'an Zhao[a,b,e,*], Yonggang Liu[e], Dawei Li[a,b], Meiping Zhu[a,b], Zhaoliang Cao[e], Jianda Shao[a,b,*], Xi Wang[f]

[a] Key Laboratory of High Power Laser Materials, Shanghai Institute of Optics and Fine Mechanics, Shanghai 201800, China
[b] Laboratory of Thin Film Optics, Shanghai Institute of Optics and Fine Mechanics, Shanghai 201800, China
[c] University of Chinese Academy of Sciences, Beijing 100039, China
[d] Shanghai Institute of Laser Plasma, Shanghai 201800, China
[e] State Key Laboratory of Applied Optics, Changchun Institute of Optics, Fine Mechanics and Physics, Changchun 130033, China
[f] State Key Laboratory of Pulsed Power Laser Technology, National University of Defense Technology, Hefei 230037, China

ARTICLE INFO

Keywords:
Near-infrared laser damage
ITO film
PI film

ABSTRACT

This report focuses on the damage characteristics of the indium-tin-oxide (ITO) layer and the polyimide (PI) layer, which are two constituent components of a LCD. This investigation is different from the previous study, in which the alignment layer was deposited directly on a glass substrate. The PI alignment layer is pinned on the ITO film to imitate the structure of the LCD as much as possible in our current study. The damage process of the ITO/Glass sample involves melting, vaporization near the laser-induced damage threshold (LIDT), and removal at a higher fluence. However, the damage process of the PI/ITO/Glass sample involves thermally induced plastic deformation, followed by cooling when the irradiation fluence is near the LIDT, and rupture when the irradiation fluence is higher. The LIDTs of the PI/ITO/Glass samples, as determined by the on-line CCD detection technique, are higher than those of the ITO/Glass samples. The favorable mechanical properties of the PI are primarily responsible for this result.

1. Introduction

Indium-tin-oxide (ITO) and polyimide (PI) films are the most commonly used transparent conductive material and alignment material for Liquid-crystal devices (LCDs),which are used in various laser systems to realize polarization control, beam shaping, wavefront correction, beam steering, etc. [1–4]. The transparent conductive layer and alignment layer are reported to be two weaker links to limit the near-infrared (IR) laser-damage-resistance of the LCD [5,6]. Usually, the LCDs used in laser systems mainly consist of glass substrate, transparent electrode, alignment and LC layers. Compared with alignment and LC layers, ITO films have been demonstrated to have much lower LIDT [5,7]. Damage in the LCD behaves as gas bubbles first. These gas bubbles are dissolved at lower fluences, while they cannot be dissolved and carbonaceous residues appear at higher fluences. It is believed that this phenomena is caused by local heating of the LC material near the ITO layers [5]. ITO films limit the LIDTs of the LCDs to serval hundreds millijoule per square centimeter under nanosecond laser irradiation at the wavelength of 1064 nm [5,7,8]. PI alignment material, which is usually used in the LCD industry has a poor near-IR laser-damage-resistance of less than 2 J/cm^2 [9].However, the laser-induced damage thresholds (LIDTs) of commercial LC materials at 1053 nm (1 ns) can reach 15 J/cm^2 [10].

Considering the lower laser-damage-resistance of ITO and PI films in the LCDs, we first focus on the damage characteristics of the ITO and the PI films irradiated using a laser with a wavelength of 1064 nm and a nanosecond pulse. In this study, the ITO film is coated with the PI alignment layer to imitate the structure of an LCD, which is different from the previous study in which the alignment layer is deposited directly on the glass substrate [5]. The effects of the PI alignment layer on the laser damage resistance of the ITO film are evaluated. The main reasons for the damage are discussed based on the observed morphologies, the distribution of the temperature field, and the mechanical properties of the PI film.

2. Sample preparation and experiments

2.1. Sample preparation

The experimental samples are denoted as ITO/Glass and PI/ITO/Glass, as illustrated in Fig. 1. The ITO films used in this study were obtained from China Southern Glass Technology (CSG) Holding Co., Ltd. The 25-nm-thick ITO films were deposited using magnetic

* Corresponding authors at: Key Laboratory of High Power Laser Materials, Shanghai Institute of Optics and Fine Mechanics, Shanghai 201800, China.
E-mail addresses: yazhao@siom.ac.cn (Y. Zhao), jdshao@mail.shcnc.ac.cn (J. Shao).

https://doi.org/10.1016/j.infrared.2019.03.028
Received 3 December 2018; Received in revised form 22 February 2019; Accepted 22 March 2019
Available online 23 March 2019
1350-4495/

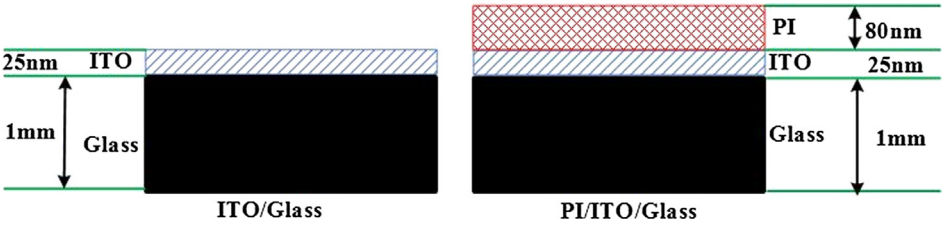

Fig. 1. Schematic of the experimental samples. The PI is pinned onto the ITO-coated glass. The thickness of the ITO layer is 25 nm; the thickness of the PI layer is 80 nm; the thickness of soda-lime glass substrate is 1 mm.

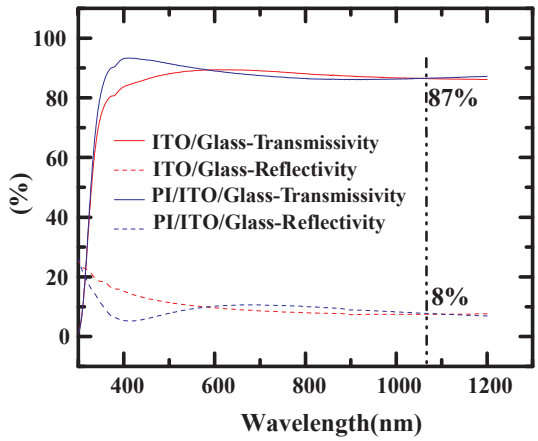

Fig. 2. Measured transmission and reflection spectra of the experimental samples.

sputtering onto 1-mm-thick soda-lime glasses. The carrier density, sheet resistance of the ITO films were measured as $1.5 \times 10^{21}/cm^3$ and 74.3 Ω/square, respectively, using an MMR Hall effect system operated at room temperature. The ITO film is polycrystalline with a strong preferred orientation of crystallite in [2 2 2] direction measured by Empyrean X-ray diffractometer. Soda-lime glass is simply referred to as glass for simplicity and its refractive index is reported to be ~1.51 [11]. For the PI/ITO/glass sample, 80-nm-thick PI films were spin-deposited from solution onto the ITO-coated glass. The PI used in this investigation is Nissan SE-5811. The thickness of the PI layer is a designed value, in addition to that of the ITO layer. The real thicknesses of the layers were checked using the step profiler and are nearly the same with the designed values. The spectral characteristics of the ITO/Glass and PI/ITO/Glass samples are shown in Fig. 2. At the wavelength of 1064 nm, the transmittance of the two samples is approximately 87%, and the reflectance is approximately 8% measured by Lambda 1050 spectrophotometer. The measured surface RMS roughness, obtained by a VEECO Dimension 3100 AFM with nanometer horizontal and vertical resolution, is ~4 nm for the ITO/Glass, and is ~3 nm for the PI/ITO/Glass. According to the relationship between the RMS roughness and the scattering [12], the scattering at 1064 nm is ~2.2‰ for the ITO/Glass, and it is ~1.3‰ for the PI/ITO/Glass. The difference is less than ~1‰, which is little and can be ignored. Therefore, the absorption of the ITO sample with the PI layer did not change significantly.

2.2. Experiments

The laser damage system used was introduced in Ref. [13]. Laser damage experiments were performed using a 12-ns pulse from a 1064 nm Nd: YAG laser at normal incidence. The model number of the laser source used is laserkids-20 and it is an early production of Beamtech Optronics Co., Ltd. The laser energy is tuned by a continuous variable attenuator comprised by a half-wave plate and a polarizer. The splitter wedge reflects one low-energy beam and EPM2000 energy meter monitors the energy of this low-energy beam. The laser is finally incident to the sample surface. In this manuscript, the laser was incident on the film surface. The effective area of the irradiation spot on the samples at normal incidence was 0.064 mm^2. A distance of 1.2 mm was used to separate two neighboring test sites. One pulse was irradiated on each test site and ten sites were tested for each fluence. The LIDT was defined as the highest fluence of the incident pulse when the damage probability was 0%. An on-line CCD detection system was used to determine the occurrence of damage. The damage morphology was initially characterized using a Leica optical microscope, and subsequently, a Zeiss scanning electron microscope (SEM) operating at an accelerated voltage of 1 kV was used to characterize detailed features of the damage. A Bruker Dektak Xt surface profiler was also used to obtain depth information of the ITO damage.

3. Results

3.1. Laser-induced damage thresholds

Three ITO/Glass and three PI/ITO/Glass samples were tested to evaluate their LIDTs. The statistical results of the LIDTs are shown in Fig. 3 and the analysis was performed using OriginPro-Data Analysis and Graphing Software. In Fig. 3, the upper line of the box represents the highest LIDT of the three samples while the bottom line represents the lowest LIDT. The middle line represents the average LIDT of the three samples. The statistical results in Fig. 3 show that the LIDTs of the PI/ITO/glass (0.7–0.8 J/cm^2) samples are higher than those of the ITO/glass (0.4–0.6 J/cm^2) samples.

3.2. Typical damage morphologies of the ITO/Glass and the PI/ITO/Glass

Two typical damage morphologies can be observed for the ITO/Glass samples using an optical microscope, as shown in Fig. 4. They are both surrounded by a light-full region. The light-full region at a lower fluence is smaller with a thicker concentric annulus, while it is larger with a thinner concentric annulus at a higher fluence. The details of these two morphologies were obtained using the SEM, as shown in Figs. 5 and 6, respectively. Fig. 5(b)–(d) show local magnified views of the micro-areas outlined by the rectangles 1, 2, and 3 in Fig. 5(a). The damage at a lower fluence near the LIDT involves melting and evaporation, as shown in Fig. 5(a). At the edge of the damage, the raised

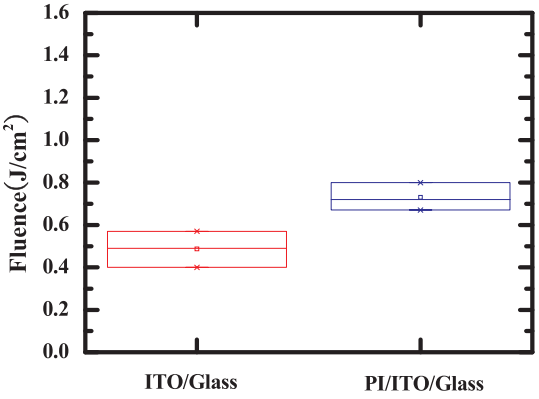

Fig. 3. LIDTs of the experimental samples. The LIDTs of PI/ITO/glass samples are higher than those of ITO/glass samples.

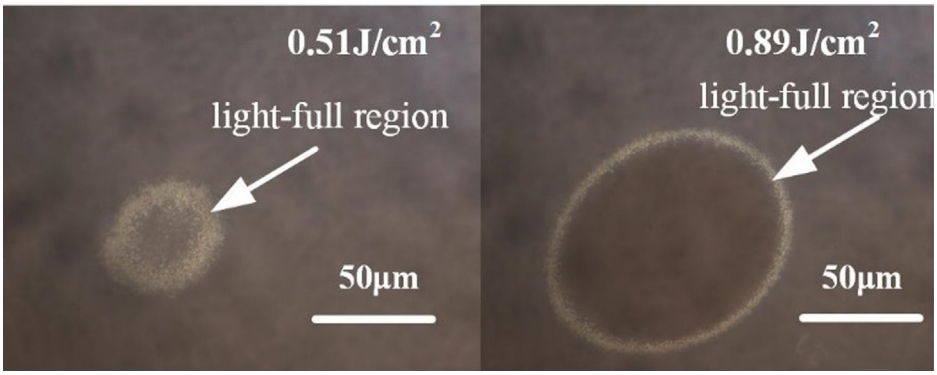

Fig. 4. Two typical damage morphologies for the ITO/Glass sample observed using optical microscopy.

melting of the ITO films can be clearly observed, as shown in Fig. 5(b). Cracks can also be observed near the outer edge of the melting region as shown in Fig. 5(c); no cracks are observed in the undamaged region, as shown in Fig. 5(d). For damage at higher fluences, the ITO film is completely removed at the center, and no damage is observed on the baked glass, as shown in Fig. 6(a). The corresponding damage-depth profile in Fig. 6(b) shows that the damage is confined to the 25-nm-thick ITO layer and that there was no damage penetration into the glass.

Typical damage morphologies for the PI/ITO/Glass sample obtained using the SEM are shown in Fig. 7. The damage process involves thermal deformation, followed by cooling after the laser pulse irradiation with a low fluence, as shown in Fig. 7(a) and (b), or rupture after the laser pulse irradiation with a high fluence, as shown in Fig. 7(c).

4. Discussions

For the ITO/Glass sample, a comparison of the optical images shown in Fig. 4 with the SEM images shown in Fig. 5 suggests that the light-full region can be attributed to the raised melting that is observed in the periphery of the damage. The phenomenon whereby the damage is confined in the ITO film indicates that the damage is associated with the ITO film rather than the glass substrate. This determined the damage morphology characteristics under the same fluence, and the melting periphery imply that the intrinsic heat absorption of the ITO films is the main damage mechanism for the ITO/Glass sample under nanosecond laser irradiation. The strong absorption induces an increase of the temperature of the ITO film. The temperature at the center of the irradiation area is the highest because the irradiating laser has a Gaussian spatial profile. When the temperature at the center is in excess of the film vaporization temperature, the ITO film is removed, and the underlying substrate is exposed. The temperature away from the center is not as high as that of this region, and may just reach the melting point of the ITO film resulting in melting. The occurrence of the crack around the melting is likely due to the rapid ITO volume change due to fast heating and cooling during film melting and resolidification processes [14].

The temperature distributions of the ITO/Glass and the PI/ITO/Glass sample were investigated based on the model described in Ref. [15]. Starting at time $t = 0$, a circularly symmetric, Gaussian beam of light propagating in the z direction illuminates the surface of multilayer as shown in Fig. 8. The number of layers is i, and, starting at the substrate with $i = 1$, the layers are numbered in increasing order. The incident intensity distribution can be written

$$I(r, t) = [P_0(t)/(\pi r_0^2)] \exp[-(r/r_0)^2] \quad (1)$$

where r_0 is the $1/e$ radius of the Gaussian beam and $P_0(t)$ is the

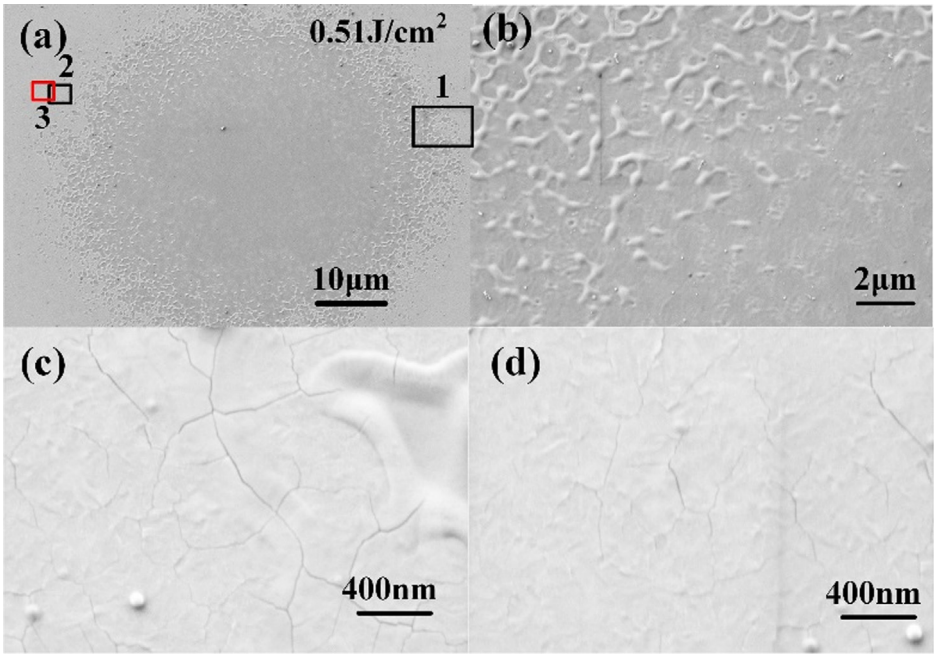

Fig. 5. Typical damage morphology of ITO/Glass at a lower fluence (near the LIDT). (b), (c), and (d) show local magnified views of micro-areas outlined by the rectangles 1, 2, and 3 in (a), respectively.

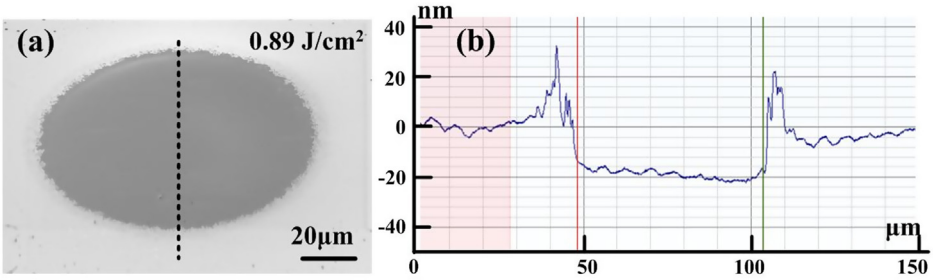

Fig. 6. (a) Typical damage morphology of the ITO/Glass sample at a higher fluence (near 100% damage probability). (b) Depth profile along the dotted line in (a).

instantaneous output power of the laser.

The laser-induced temperature distribution is determined by the absorption of the laser energy and heat transfer processes, which can be expressed as follows:

$$C_i(\partial/\partial t)T(r, z, t) - K_i\nabla^2 T(r, z, t) = g(r, z, t); \quad (2)$$

$$(\partial/\partial t)T(r, z = 0, t) = \gamma T(r, z = 0, t); \quad (3)$$

$$T(r, z = \infty, t) = T(r = \infty, z, t) = 273\,\mathrm{K}; \quad (4)$$

$$T(r, z, t = 0) = 273\,\mathrm{K} \quad (5)$$

Where C_i and K_i are the specific heat and heat conductivity of the i_{th} layer respectively, γis a constant which controls the rate of the heat flow from the surface of the coatings, T(r, z, t) is the temperature at point (r, z) and time t, and g(r, z, t) is the absorption rate of the energy per unit volume per unit time at z. The heat loss from the surface is assumed to be proportional to T(r, z = 0, t) and the proportionality constant γ is chosen to be 10^5/cm which makes the convection losses be of the same order of magnitude as the heat losses to the substrate according to Ref. [15] in our calculation. The average amount of power per unit area that crosses the plane perpendicular to the Z axis at z can be written

$$g(r, z, t) = d[I(r, t)Y(z)]/dz \quad (6)$$

Where $Y(z) = \mathrm{Re}[1/2E(z)\cdot H^*(z)]$, the electric field $E(z)$ and magnetic field $H(z)$ can be obtained from Maxwell equations.

The numerical solutions of the heat transfer equation (Eq. (2)) can be obtained by separately applying the 1-D implicit technique, which is called the alternating direction implicit technique. In this technique, the time step Δt is divided into two equal half steps, 1/2△t each. In going from $k\Delta t$ to $(k + 1/2)\Delta t$, r is treated explicitly and z is treated implicitly; in going from $(k + 1/2)\Delta t$ to $(k + 1)\Delta t$, z is treated explicitly and r is treated implicitly. A more detailed description of this model is presented in Ref. [15]. All of the thermal parameters of the films and the substrate used for the numerical calculations are listed in Table 1. The absorption coefficient in Table 1 of the ITO film is obtained from the Beer-Lambert law,

$$\alpha(\lambda) = \left(-\frac{1}{d}\ln\left[\frac{T(\lambda)}{(1 - R(\lambda))(1 - R'(\lambda))}\right]\right)$$

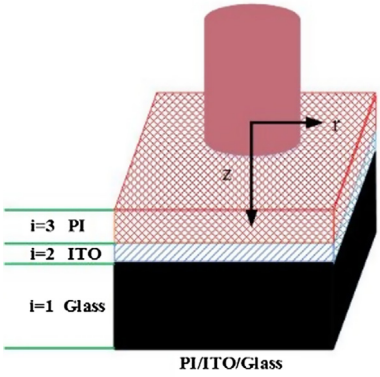

Fig. 8. A circularly symmetric Gaussian beam of light, propagating in the z direction, illuminates the surface. The axis of symmetry for the beam is r = 0.

Table 1
Summary of parameters used for the temperature distribution calculations.

Material parameter	Glass	ITO	PI
Refractive index	1.51[a]	1.96[b]	1.59[c]
Absorption coefficient (/m)	0	1×10^6	0[d]
Specific heat (J/cm³/K)	2.00	2.43[b]	1.55[c]
Heat conductivity (W/cm/K)	0.0140	0.1100[b]	0.003[e]
Thickness (nm)	1000	25	80

[a] From Appl. Opt. 41, 2888 (2002).
[b] From Opt. Express 25, 25533 (2017).
[c] From Appl. Phys. A-Mater. Sci. Process. 80, 529 (2005).
[d] From Appl. Phys. B-Lasers Opt. (2018).
[e] From J. Microelectromech. Syst. 8, 180 (1999).

Where d is the thickness of the ITO film, $T(\lambda)$ is the measured transmission of the ITO/Glass sample, $R(\lambda)$ is the measured reflectivity of the ITO/Glass sample, $R'(\lambda)$ is the estimated reflectivity between the ITO on glass interface is $R'(\lambda)$ given by $R'(\lambda) = [(n_{ITO} - n_{\mathrm{glass}})/(n_{ITO} + n_{\mathrm{glass}})]^2$, where n_{ITO} is the refractive index of ITO, and n_{glass} is the refractive index of glass. The calculated absorption coefficient of the ITO film is $\sim 1 \times 10^6$/m, which is nearly the same as the value reported in a previous report [16].

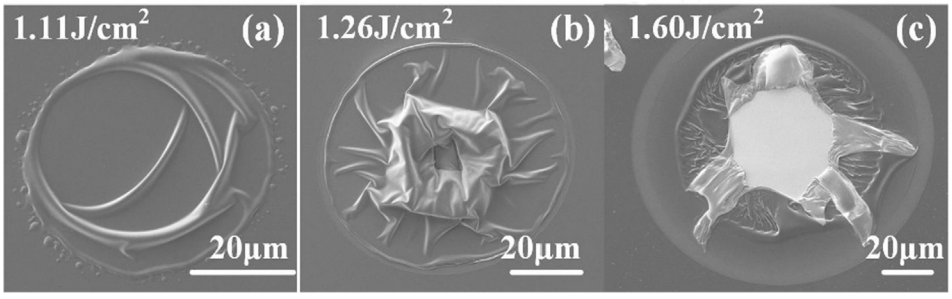

Fig. 7. Typical damage morphologies of the PI/ITO/Glass sample.

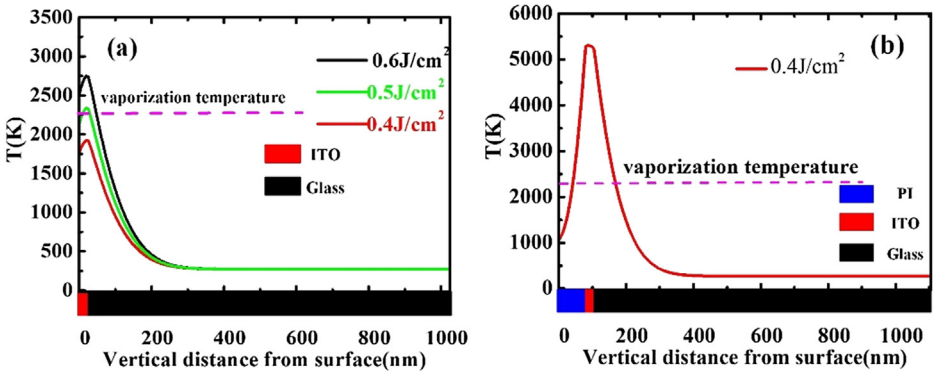

Fig. 9. Temperature distribution of the irradiated center in the samples. The dashed lines represent the vaporization temperature of the ITO film.

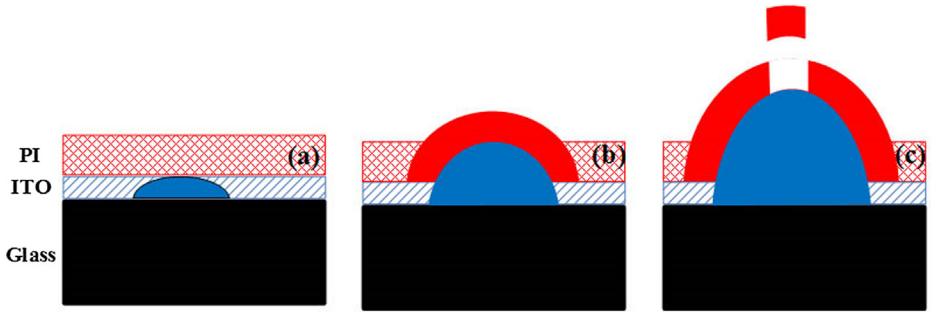

Fig. 10. Schematic representation of the damage process of PI/ITO/Glass.

The calculated temperature distributions at the irradiated center of the ITO/Glass sample are shown in Fig. 8(a). The temperature distributions from the ITO surface to the glass are induced by fluences of 0.4, 0.5, and 0.6 J/cm^2 and the presented values represent the maximum temperature during a 12-ns Gaussian laser pulse. Fig. 8 (a) shows that the peak temperature in the ITO film reaches ~2000 K at a fluence of 0.4 J/cm^2 and ~2800 K at 0.6 J/cm^2. The vaporization temperature of the ITO film reported in the literature is ~2200 K [14,17]. As such, the calculated temperature results for the irradiated center prove that the temperature of the ITO film induced by its absorption of the pulsed laser energy, exceeds the film's vaporization temperature. In this case, the damage is caused by melting and vaporization.

The temperature distribution at the irradiated center of the PI/ITO/Glass sample induced by a fluence of 0.4 J/cm^2 is shown in Fig. 8 (b). The temperature in the ITO layer is shown to be higher than that of the PI layer and glass and the melting or evaporation temperature of PI exceeds 3000℃ [18,19], which suggests that the damage process for the PI/ITO/Glass can be illustrated as shown in Fig. 9. The ITO underlayer first absorbs heat under laser irradiation and this process is followed by melting and vaporization as shown in Fig. 9 (a). Only when the pressure induced by the melting or vaporizing of the ITO layer is sufficiently large to reach the yield strength of the PI film, and it begins to undergo plastic deformation. The plastic deformation leads to the surface rise represented in Fig. 9 (b), and morphological damage is observed. The morphology of the damage shown in Fig. 7 indicates that the pressure induced by the melting or evaporation of the ITO layer is not sufficiently high to break the surface PI at lower fluences. After the laser shot, the rising plastic deformation cools down, which results in the damage morphologies shown in Fig. 7(a) and (b). A higher-fluence irradiation induces a larger pressure, leading to a larger thermally induced plastic deformation. The larger pressure could easily exceed the tensile strength of the PI film, leading to a rupture as shown in Fig. 7(c).

Compared with Fig. 8 (a) and Fig. 8 (b), the temperature rise of the ITO layer for the PI/ITO/Glass is higher than that for the ITO/Glass for the same fluence. The lower thermal conductivity of the PI film may be responsible for this result. Due to the lower thermal conductivity of PI compared with that of the ITO film, the heat induced by the underlayer ITO film cannot be transferred to the PI film effectively, leading to a lower temperature on the PI/ITO/Glass surface than that on the ITO/Glass surface. Therefore, heat convective loss from the surface for the PI/ITO/Glass sample, is less effective than that for the ITO/glass sample and finally contributes to a higher temperature of the ITO film for the PI/ITO/Glass sample. However, it must be noted that there will be a significant difference between the actual and calculated temperature values of the PI/ITO/Glass sample for a fluence of 0.4 J/cm^2. This is because the proposed temperature model is correct when the film is in a solid state. However, the model is incorrect for temperature rise calculations after melting and vaporization of the ITO film. There are two main reasons that account for the difficulty in providing reliable temperature values at present. The first is that the thermal parameters of the ITO film shown in Table 1 change significantly after ITO vaporization. The other is that the ITO gas experiences an expansion cooling process as it is heated further (see Fig. 10).

The temperature of the ITO layer for the PI/ITO/Glass is higher than that of the ITO/Glass induced by the same fluence. However, the LIDT of the PI/ITO/Glass is shown to be higher than that of the ITO/Glass. A possible explanation is that ITO vaporization occurs at a lower value than that of the measured LIDT fluence. However, no plastic deformation damage can be observed on the surface of the PI film because the pressure of the vaporized ITO is lower than the yield strength of the PI film. The mechanical properties of the PI are favorable and it has been reported that the measured yield strength of the PI layer can reach ~300 MPa [20]. Therefore, it is possible that no plastic deformation damage can be observed when the ITO film begins to vaporize. After irradiation, the ITO gas which is confined between the PI film and the glass cools and redeposits. It is very difficult for the on-line CCD to identify this change. Irradiation at a fluence higher than the critical fluence induced initial vaporization of the ITO film, the ITO layer can further absorb heat after vaporization, leading to a pressure greater than that of initial vaporization of the ITO. If the pressure is large enough to exceed the yield stress of the PI layer, then plastic deformation damage can be observed using the on-line CCD detection technique.

The acquired mechanical properties of the PI are responsible for the LIDT result of the PI/ITO/Glass.

5. Conclusions

The damage characteristics of ITO/Glass and PI/ITO/Glass were investigated. The main experimental conclusions are as follows:

(1) The damage process of the ITO/Glass sample involves melting, vaporization near the LIDT, and removal at a higher fluence. The damage is confined in the ITO film; it did not penetrate into the glass. The damage of the ITO/Glass sample is attributed to the high absorption of the ITO film.
(2) The damage process of the PI/ITO/Glass involves thermally induced plastic deformation, followed by cooling when the irradiation fluence is low, and rupture when the irradiation fluence is high. The damage in the PI/ITO/Glass sample is determined by the competition between the pressure induced by the ITO vaporization and the mechanical properties of the PI film.
(3) The temperature of the ITO layer for the PI/ITO/Glass is higher than that for the ITO/Glass induced by the same fluence. However, the LIDIs as determined by the on-line CCD detection technique are higher for the PI/ITO/Glass samples than those of the ITO/Glass. The possible reason is that the ITO film experienced vaporization below the LIDT fluence of the PI/ITO/Glass. No plastic deformation damage can be observed on the surface of the PI film because the pressure of the vaporized ITO is lower than the yield strength of the PI film. The favorable mechanical properties of the PI is responsible for the LIDT result of the PI/ITO/Glass.

Conflicts of interest

The authors declared that they have no conflicts of interest to this work.

Funding

This work is supported by National Natural Science Foundation of China (NSFC) (11874369, 61308021 and 11774319) and Open Research of Fund of State Key Laboratory of Pulsed Laser Technology.

Acknowledgments

The authors would like to thank Professor Zhengxiu Fan for the helpful discussions.

References

[1] S.D. Jacobs, K.A. Cerqua, K.L. Marshall, A. Schmid, M.J. Guardalben, K.J. Skerrett, Liquid-crystal laser optics-design, fabrication, and performance, J. Opt. Soc. Am. B-Opt. Phys. 5 (1988) 1962–1979.
[2] D. Huang, W. Fan, H. Cheng, G. Xia, L. Pei, X. Li, Z. Lin, Wavefront control of laser beam using optically addressed liquid crystal modulator, High Power Laser Sci. Eng. 6 (2018) e20.
[3] J. Beeckman, K. Neyts, P.J.M. Vanbrabant, Liquid-crystal photonic applications, Opt. Eng. 50 (2011) 081202.
[4] L. Wu, X.R. Wang, C.D. Xiong, Z.Q. Huang, R.S. Zhuo, J.R. Rao, Q.G. Tan, Polarization-independent two-dimensional beam steering using liquid crystal optical phased arrays, Chin. Opt. Lett. 15 (2017) 101601.
[5] F.L. Vladimirov, N.I. Pletneva, L.N. Soms, V.P. Pokrovskiy, Laser-damage resistance of the liquid crystal modulators, Mol. Cryst. Liq. Cryst. Sci. Tech. Mol. Cryst. Liq. Cryst. 321 (1998) 213–221.
[6] K.L. Marshall, D. Saulnier, H. Xianyu, S. Serak, N. Tabiryan, Liquid crystal near-IR laser beam shapers employing photoaddressable alignment layers for high-peak-power applications, Proc. SPIE 8828 (2013) 88280N.
[7] Z. Raszewski, W. Piecek, L. Jaroszewicz, L. Soms, J. Marczak, E. Nowinowski-Kruszelnicki, P. Perkowski, J. Kedzierski, E. Miszczyk, M. Olifierczuk, P. Morawiak, R. Mazur, Laser damage resistant nematic liquid crystal cell, J. Appl. Phys. 114 (2013) 053104.
[8] Z. Raszewski, W. Piecek, L. Jaroszewicz, R. Dabrowski, E. Nowinowski-Kruszelnicki, L. Soms, M. Olifierczuk, J. Kedzierski, P. Morawiak, R. Mazur, E. Miszczyk, M. Mrukiewicz, K. Kowiorski, Transparent laser damage resistant nematic liquid crystal cell "LCNP3", Opto-Electron. Rev. 22 (2014) 196–200.
[9] K.L. Marshall, J. Gan, G. Mitchell, S. Papernov, A.L. Rigatti, A.W. Schmid, S.D. Jacobs, Laser-damage-resistant photoalignment layers for high-peak-power liquid crystal device applications, Proc. SPIE 7050 (2008) 70500L.
[10] S.D. Jacobs, K.A. Cerqua, K.L. Marshall, A. Schmid, M.J. Guardalben, K.J. Skerrett, Liquid-crystal laser o ptics: design, fabrication, and performance, J. Opt. Soc. Am. B 5 (1988) 1962–1979.
[11] A. Belkhir, Detailed study of silver metallic film diffusion in a soda-lime glass substrate for optical waveguide fabrication, Appl. Opt. 41 (2002) 2888–2893.
[12] H.E. Bennett, J.O. Porteus, Relation between surface roughness and specular reflectance at normal incidence, J. Opt. Soc. Am. 51 (1961) 123–129.
[13] W.W. Liu, C.Y. Wei, J.B. Wu, Z.K. Yu, H. Cui, K. Yi, J.D. Shao, Investigations on single and multiple pulse laser-induced damages in HfO_2/SiO_2 multilayer dielectric films at 1064 nm, Opt. Express 21 (2013) 22476–22487.
[14] J.-H. Yoo, M.G. Menor, J.J. Adams, R.N. Raman, J.R.I. Lee, T.Y. Olson, N. Shen, J. Suh, S.G. Demos, J. Bude, S. Elhadj, Laser damage mechanisms in conductive widegap semiconductor films, Opt. Express 24 (2016) 17616–17634.
[15] M. Mansuripur, G.A. Neville Connell, J.W. Goodman, Laser induced local heating of multilayers, Appl. Opt. 21 (1982) 1106–1114.
[16] C. McDonnell, D. Milne, C. Prieto, H. Chan, D. Rostohar, G.M. O'Connor, Laser patterning of very thin indium tin oxide thin films on PET substrates, Appl. Surf. Sci. 359 (2015) 567–575.
[17] O. Yavas, M. Takai, Effect of substrate absorption on the efficiency of laser patterning of indium tin oxide thin films, J. Appl. Phys. 85 (1999) 4207–4212.
[18] B. Nysten, J.C. Roux, S. Flandrois, C. Daulan, H. Saadaoui, AFM and STM studies of the carbonization and graphitization of polyimide film, Phys. Rev. B 48 (1993) 12527–12538.
[19] A.K. Shukla, V.M. Yadav, A. Kumar, I.A. Palani, A. Manivannan, Investigations on effect of laser-induced self-assembled patterning on optical properties of flexible polyimide substrates for solar cell applications, J. Phys. D: Appl. Phys. 51 (2018) 045502.
[20] H. Kikuchi, J.A. Logan, D.Y. Yoon, Study of local stress, morphology, and liquid-crystal alignment on buffed polyimide surfaces, J. Appl. Phys. 79 (1996) 6811–6817.